Inorganic Chemistry

Article

pubs.acs.org/IC

Efficient Förster Resonance Energy Transfer in 1,2,3-Triazole Linked BODIPY-Zn(II) Meso-tetraphenylporphyrin Donor–Acceptor Arrays

Matthew J. Leonardi,† Michael R. Topka, and Peter H. Dinolfo*

Department of Chemistry and Chemical Biology, Rensselaer Polytechnic Institute, 110 Eighth Street, Troy, New York 12180, United States

Supporting Information

ABSTRACT: Cu(I) catalyzed azide–alkyne cycloaddition (CuAAC) reactivity was successfully employed to synthesize three donor–acceptor energy transfer (EnT) arrays that contain one (**Dyad**), three (**Tetrad**) and four (**Pentad**) 4,4-difluoro-4-bora-3a,4a-diaza-s-indacene (BODIPY) donors connected to a Zn-tetraphenylporphyrin acceptor via 1,2,3-triazole linkages. The photophysical properties of the three arrays, along with individual donor and acceptor chromophores, were investigated by UV–vis absorption and emission spectroscopy, fluorescence lifetimes, and density functional theory (DFT) electronic structure modeling. Comparison of the UV–vis absorption spectra and frontier molecular orbitals from DFT calculations of the three arrays with **ZnTPP**, **ZnTTrzlP**, and **Trzl-BODIPY** shows that the electronic structure of the chromophores is essentially unperturbed by the 1,2,3-triazole linkage. Time-dependent DFT (TDDFT) calculations on the **Dyad** reproduce the absorption spectra in THF and show no evidence of excited state mixing of the donor and acceptor. The BODIPY singlet excited state emission is significantly quenched in all three arrays, consistent with EnT to the porphyrin core, with efficiencies of 95.8, 97.5, and 97.2% for the **Dyad**, **Tetrad**, and **Pentad**, respectively. Fluorescence excitation spectra of the three arrays, measured at the porphyrin emission, mirror the absorption profile of both the porphyrin and BODIPY chromophores and are consistent with the Förster resonance energy transfer (FRET) mechanism. Applying Förster theory to the spectroscopic data of the chromophores gives EnT efficiency estimates that are in close agreement with experimental values, suggesting that the through-space mechanism plays a dominant role in the three arrays.

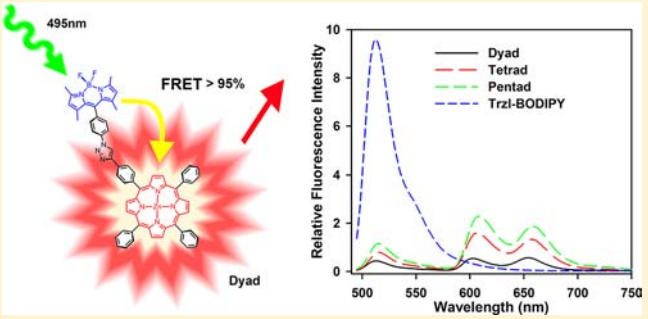

INTRODUCTION

The utilization of molecular systems for solar energy conversion requires the rational design and synthesis of chromophoric arrays that can absorb light across a large fraction of the solar spectrum and direct that energy toward catalytic sites for chemical fuel generation, or semiconductor electrode surfaces for electrical charge production.[1−5] The development of efficient light harvesting systems that mimic the natural photosynthetic apparatuses requires a fundamental understanding of the structural–functional relationship between the various donor and acceptor chromophores.

Molecular chromophore-based energy transfer arrays have often employed porphyrin building blocks due to their structural resemblance to chlorophylls found in natural photosynthetic systems. Additionally, porphyrins are relatively easy to synthesize while providing somewhat straightforward methods to tune their photophysical and redox properties. Porphyrins are often characterized by their strong, but localized, absorption bands in the blue and red regions of the visible spectrum, Soret and Q-bands respectively, yet they lack a significant optical cross section for a large fraction of the visible spectrum (green light, 450–550 nm). Thus, even though porphyrins have found use in several applications related to solar energy harvesting (photovoltaics, DSSCs, etc.), they are not ideally suited for broad-band solar harvesting.

Toward the goal of using porphyrins in broad-band light harvesting, there have been numerous examples of donor–acceptor array complexes created where green absorbing chromophores have been coupled to porphyrins to create energy transfer arrays that improve overall broad-band light harvesting. One of the common green chromophore donors used for this purpose is 4,4-difluoro-4-bora-3a,4a-diaza-s-indacene, or BODIPY.[6] This complex exhibits strong molar absorbtivities in the 400–500 nm range ($\sim 5 \times 10^5$ M^{-1} cm^{-1}), relatively long-lived singlet excited states, and high quantum yields for singlet fluorescence.[7] Additionally, synthetic modification of the pyrrole groups allows for some tuning of the singlet $\pi-\pi^*$ transition energies.[7] The fluorescence emission overlaps with ZnTPP Q-bands, which allows for efficient Förster resonance energy transfer (FRET). Additionally, the BODIPY $\pi-\pi^*$ absorption band is usually isolated from porphyrin Soret & Q-bands, allowing for selective excitation of the donor to quantify FRET. There have been a number of

Received: June 1, 2012
Published: December 6, 2012

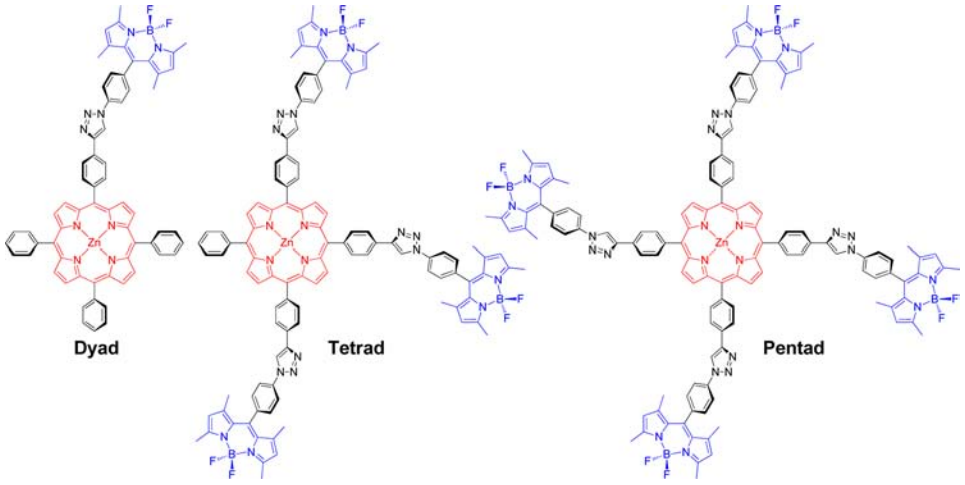

Figure 1. BODIPY-porphyrin donor–acceptor arrays.

Scheme 1. Synthetic Schemes for the Arrays and Individual Chromophores

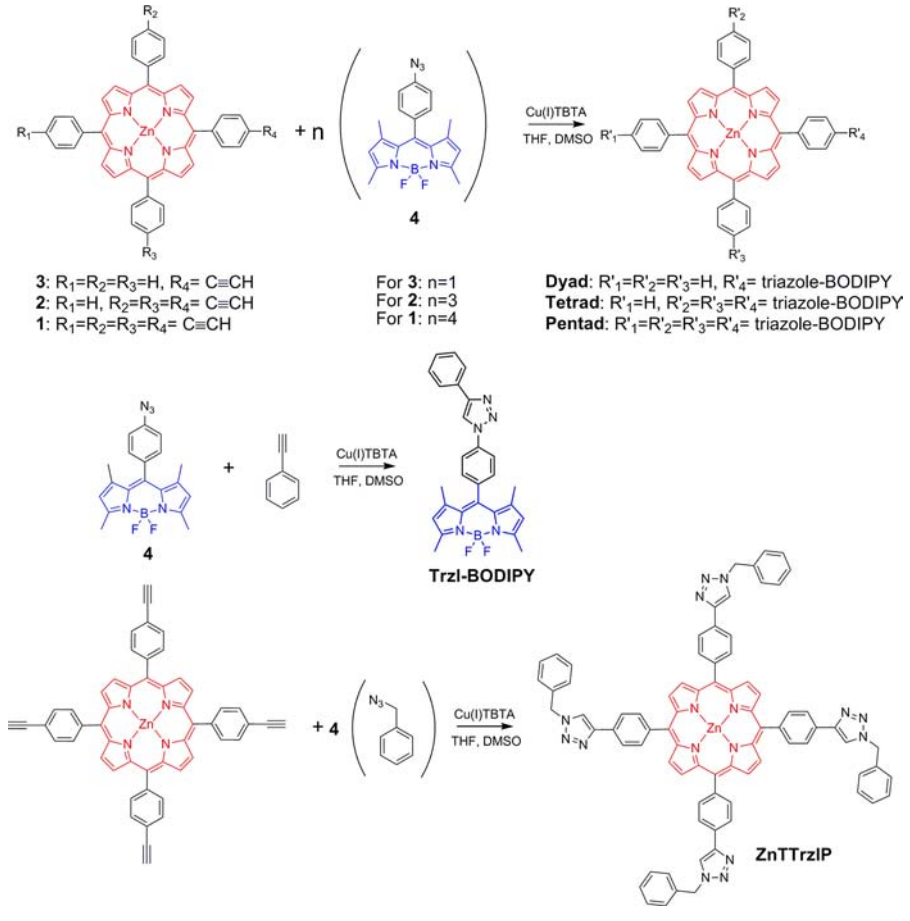

reports on BODIPY-porphyrin donor–acceptor architectures that utilize a range of coupling methodologies, including covalent connections,[8–16] noncovalent self-assembly,[11,17] and metal–organic frameworks.[18] Several of these molecular arrays have also been incorporated into dye-sensitized semiconductor solar cells to improve overall light harvesting ability of the photoelectrochemical cell.[15,16] Generally, these energy transfer (EnT) systems result in high FRET efficiency (>90%) from the BODIPY donor to the porphyrin acceptor due to favorable spectral overlap, with the largest variations stemming from the differences in intermolecular distance and orientation of the chromophores afforded by the coupling group.

We have been interested in the utilization of copper(I) catalyzed azide–alkyne cycloaddition (CuAAC) reactivity[19–21] to assemble multilayer thin-films of 5,10,15,20-*tetra*(4-ethynylphenyl)porphyrin Zn(II) on electrode surfaces for various photoelectrochemical applications.[22–25] Toward that goal, we wish to explore the utility of CuAAC reactivity to assemble molecular donor–acceptor systems and examine the influence of the 1,2,3-triazole linkage on photophysical

dx.doi.org/10.1021/ic301170a | *Inorg. Chem.* 2012, 51, 13114–13122

processes, such as EnT, between adjacent chromophores. CuAAC is an attractive covalent coupling method for assembling molecular donor−acceptor systems due to its high synthetic yield, mild reaction conditions, and tolerance of other functional groups.[19−21] Additionally, the 1,4-substituted 1,2,3-triazole provides a stable and rigid linker between adjacent groups. We have shown previously that 5,10,15,20- *tetra*-(4-ethynylphenyl)porphyrin Zn(II) (**1**) is a successful synthon in CuAAC reactivity for creation of molecular multilayer films on a variety of substrates.[22−25] Therefore, we chose to explore its solution reactivity with the azido functionalized BODIPY, 4,4-difluoro-8-(4-azidophenyl)-1,3,5,7-tetramethyl-4-bora-3a,4a-diaza-*s*-indacene (**4**). Herein, we report on the synthesis and photophysical characterization of three EnT arrays that contain one (**Dyad**), three (**Tetrad**), and four (**Pentad**) BODIPY donors connected to a Zn-tetraphenylporphyrin acceptor via 1,4-subsitituted 1,2,3-triazole linkages (Figure 1). The 1,2,3-triazole linkages provide a rigid, covalent connection that allows for efficient FRET between chromophores (>95%), while minimizing through-bond orbital overlap. Applying Förster theory[26] to the spectral data estimates EnT efficiencies that are in close agreement with measured values from fluorescence quenching of the BODIPY donors in the three arrays.

RESULTS AND DISCUSSION

Synthesis. Scheme 1 shows the synthetic methodology for the three 1,2,3-triazole linked BODIPY-porphyrin arrays examined in this study, along with individual chromophores used for comparison. The EnT arrays utilize meso-5,10,15,20-*tetra*-phenylporphyrin Zn(II) as the core acceptor and one (**Dyad**), three (**Tetrad**), and four (**Pentad**) BODIPY donors attached at the para-position of the meso-phenyl rings. The arrays were synthesized from ethynyl modified porphyrins and azido-BODIPY building blocks using standard CuAAC conditions.[21] The unoptimized CuAAC reaction conditions used in this study gave yields of 65%, 16%, and 48% for the **Dyad**, **Tetrad**, and **Pentad** respectively. Upon investigation of side products from these reactions, it was determined that they consisted primarily of porphyrins containing unreacted ethynyl groups. The resulting 1,2,3-triazole linked arrays are easily separated from minor side products using preparatory-scale thin layer chromatography. NMR spectra of the compounds show a clear combination of the porphyrin and BODIPY signals. The phenyl protons on the BODIPY are shifted downfield due to the presence of the electron-withdrawing triazole, and the porphyrin ethynyl proton at 3.4 ppm changes to a 1,2,3-triazole signal, which is shifted downfield to ∼8.6 ppm in all three arrays. This shift in the position of the ethynyl proton provides confirmation that the CuAAC reaction occurred. Additionally, UV−vis absorption spectra, ^{1}H NMR, and mass spectra of the reaction solutions revealed that Cu(II) insertion into the porphyrin from the CuAAC catalyst did not occur in any detectable amount.

In addition to the BODIPY-porphyrin arrays, we synthesized 5,10,15,20-*tetra*-(*p*-benzyl-1,4-triazolephenyl)porphyrin Zn(II) (**ZnTTrzlP**) and 4,4-difluoro-8-(4-(phenyl-1,4-triazole)-phenyl)-1,3,5,7-tetramethyl-4-bora-3a,4a-diaza-*s*-indacene (**Trzl-BODIPY**) as photophysical standards for the individual donor and acceptor chromophores with attached 1,2,3-triazoles. These were synthesized using the same CuAAC conditions[21] as the arrays (Scheme 1).

Electronic Absorption. The top of Figure 2 shows the absorption spectra for individual chromophores **ZnTTrzlP** and **Trzl-BODIPY** in THF. The absorption spectra for the **Dyad**, **Tetrad**, and **Pentad** in THF are shown at the bottom of Figure 2. The **Dyad** displays the expected porphyrin Soret and Q-bands at 424, 556, and 596 nm, in addition to the BODIPY $\pi-\pi^*$ transition at 503 nm.[27,28] The absorption spectrum of the **Dyad** is simply a summation of the individual chromophores (**ZnTPP** and **Trzl-BODIPY**) and does not show any new bands or broadening of the base peaks, suggesting that electronic mixing between chromophores is minimal or nonexistent. The absorption spectra of the **Tetrad** and **Pentad** are very similar to that of the **Dyad**, with the expected increase in the BODIPY $\pi-\pi^*$ transition, roughly three and four times larger for **Tetrad** and **Pentad**, respectively. The **Tetrad** and **Pentad** also show a slight red-shift (3−4 nm) of the porphyrin Soret and Q-band peaks relative to **ZnTPP** due to the electron withdrawing effects of the 1,2,3-triazoles on the *meso*-phenyl rings.[29] This is consistent with the absorption spectrum of **ZnTTrzlP**, which also shows a 3−4 nm red-shift in the Soret and Q-band peaks relative to **ZnTPP**. The absorption spectra of **ZnTPP** and **ZnTTrzlP** lack any significant absorption intensity in the region from 450 to 530 nm, thus allowing for selective excitation of the BODIPY donor chromophore for examination of EnT processes.

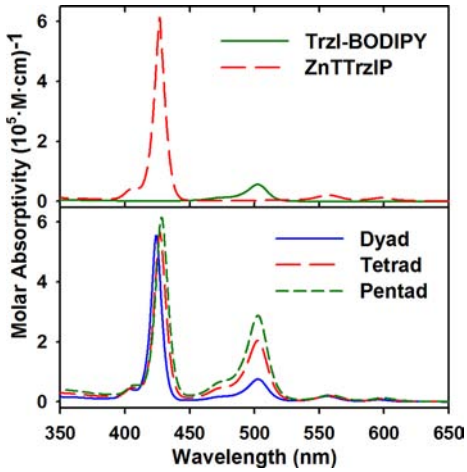

Figure 2. Top: Absorption spectra of Trzl-BODIPY and ZnTTrzlP (solid green and dashed red lines) in THF. Bottom: Absorption spectra of the **Dyad**, **Tetrad**, and **Pentad** (solid blue, long dashed red, and short dashed green lines) in THF.

Steady-State Emission. Figure 3 shows the absorption spectra of **ZnTTrzlP** and **Trzl-BODIPY**, along with the emission spectrum of **Trzl-BODIPY**. The emission of **Trzl-BODIPY** has good overlap with Q-band absorptions of **ZnTTrzlP** (signified by the shaded region), setting up a favorable situation for efficient FRET between chromophores. The emission spectra of the **Dyad**, **Tetrad**, and **Pentad** in THF, excited close to the maximum of the BODIPY $\pi-\pi^*$ transition at 495 nm, are shown in Figure 4. The spectra show some fluorescence from the BODIPY chromophore in the region from 500 to 550 nm, but also the emission bands from Zn porphyrin core at 605 and 660 nm. Since neither **ZnTPP** or **ZnTTrzlP** absorbs significantly at 495 nm, the porphyrin emission must be the result of EnT from the BODIPY donor. Fluorescence excitation spectra also show the presence of singlet−singlet energy transfer from BODIPY to porphyrin. Figure 5 shows the excitation spectra of equimolar solutions of the three arrays in THF, measuring $S_1 \rightarrow S_0$ fluorescence of the

dx.doi.org/10.1021/ic301170a | *Inorg. Chem.* 2012, 51, 13114−13122

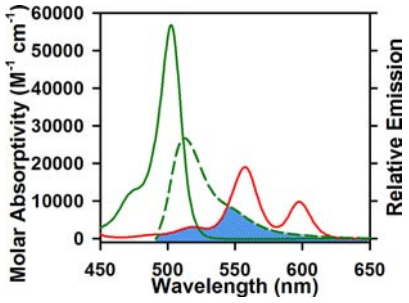

Figure 3. Absorption spectra of the **Trzl-BODIPY** and **ZnTTrzlP** (solid green and red lines respectively) in THF. The emissions spectrum of **Trzl-BODIPY** in THF is shown as a dashed green line (excitation at 502 nm) and has been normalized to the absorption spectra by the quantum yield for singlet fluorescence (φ = 0.47). The overlap between the emission of **Trzl-BODIPY** and the Q-band absorptions of **ZnTTrzlP** is shaded in blue.

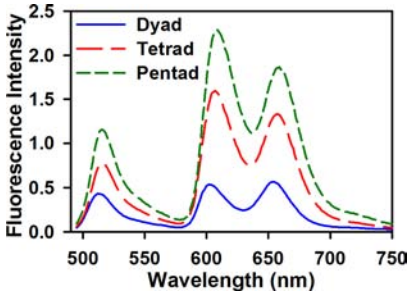

Figure 4. Emission spectra of equimolar solutions of the **Dyad** (solid blue line), **Tetrad** (long dashed red line), and **Pentad** (short dashed green line) in THF, excited close to the maximum of the BODIPY $\pi-\pi^*$ transition at 495 nm.

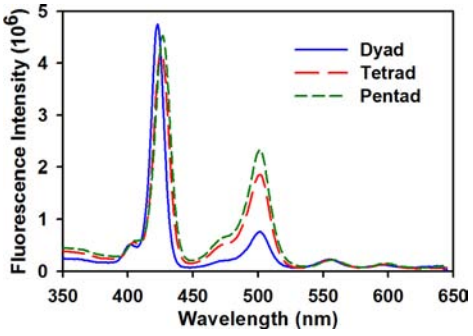

Figure 5. Excitation spectra of equimolar solutions of the **Dyad** (solid blue line), **Tetrad** (long dashed red line), and **Pentad** (short dashed green line) in THF, observing the $S_1 \rightarrow S_0$ fluorescence of the Zn porphyrin core at 660 nm.

porphyrin at 660 nm. The spectra show excitation bands for the porphyrin Soret and Q-bands as in free **ZnTPP**, as well as the BODIPY $\pi-\pi^*$ transition at 495 nm. These spectra show a linear increase in the amount of excitation intensity at 495 nm with increasing BODIPY units, consistent with the absorption spectra and number of donor chromophores attached to the porphyrin acceptor.

Table 1 contains spectroscopic data of the arrays and control complexes. The quantum yield of 1,3,5,7-tetramethyl-8-phenyl-4,4-difluoroboradiazaindacene (**Ph-BODIPY**) in THF has been reported previously as 0.72.[30] We observed a decrease in quantum yield for **Trzl-BODIPY** to 0.47 following 1,2,3-triazole formation at the *para* position on the phenyl ring. Electron withdrawing groups on the *para* position of the phenyl ring have been shown to decrease quantum yield of BODIPY chromophores.[31] The moderate decrease in quantum yield suggests that the N1 position of the 1,2,3-triazole induces a small electron withdrawing effect in this application. The quantum yield for **ZnTTrzlP** (0.047) shows a slight increase over the reported value for **ZnTPP** (0.032) in THF.[32] When electron donating groups are attached at the *para* position on the phenyl ring, the quantum yield of **ZnTPP** increases by putting more electron density into the porphyrin ring current.[33,34] The C4 position of the 1,2,3-triazole ring has been shown to have a slight electron donating effect in photophysical applications.[35]

The quantum yield (ϕ) for $S_1 \rightarrow S_0$ fluorescence of the Zn porphyrin core for the arrays, **Dyad**, **Tetrad**, and **Pentad**, were determined from excitation of the BODIPY donor and thus include the yield of EnT to the porphyrin acceptor. The quantum yields for the EnT arrays are consistent with emission from the porphyrin core and suggest that EnT from the BODIPY is relatively efficient and fast. Additionally, the values increase somewhat from the **Dyad** (0.033), to **Tetrad** (0.039) and **Pentad** (0.041) and are consistent with the trend between the **ZnTPP** and **ZnTTrzlP** standards. The addition of 1,2,3-triazole linkages to the ZnTPP core via the para-phenyl position adds slightly to the electron donating ability of the phenyl rings and increases the quantum yield for $S_1 \rightarrow S_0$ fluorescence of the Zn porphyrin core.

Fluorescence Lifetimes. Fluorescence lifetimes were measured for all arrays, as well as for **ZnTPP**, **ZnTTrzlP**, and **Trzl-BODIPY**, and are shown in Table 1. The arrays showed fluorescence lifetimes that closely matched that of **ZnTPP** at around 1.8 ns. This suggests that singlet−singlet energy transfer from the BODIPY to the porphyrin occurs at a very fast rate so that the porphyrin lifetime is the limiting factor for the rate of fluorescence. This ties in with the previously stated efficiencies of energy transfer, as a faster energy transfer rate leads to a

Table 1. Summary of Spectroscopic Data for the Arrays and Control Complexes

	absorption	emission		
compound	λ_{max} / nm (ε/M^{-1}cm^{-1})	λ_{max} / nm	ϕ	τ_F (ns)
Trzl-BODIPY	503 (56,000)	513	0.47 ± 0.02	2.67 ± 0.02
ZnTTrzlP	427 (612,000); 557 (20,000); 598 (11,000)	608; 659	0.047 ± 0.001	1.76 ± 0.01
ZnTPP	424 (623,000); 556 (20,100); 594 (9,100)	602; 652	0.032[a]	1.91 ± 0.03[b]
Dyad	424 (554,000); 503 (75,000); 556 (18,500); 596 (6,800)	513; 603; 654	0.033 ± 0.001[c]	1.96 ± 0.01[c]
Tetrad	427 (564,000); 503 (204,000); 558 (19,500); 598 (9,900)	515; 607; 657	0.039 ± 0.002[c]	1.82 ± 0.01[c]
Pentad	428 (613,000); 503 (287,000); 559 (22,000); 599 (12,500)	515; 608; 659	0.041 ± 0.001[c]	1.79 ± 0.02[c]

[a]Data taken from ref 32. [b]This is compared to a value of 1.87 ns taken from ref 36. [c]Data obtained via excitation of BODIPY donor and include yield of EnT to the porphyrin acceptor (see text).

dx.doi.org/10.1021/ic301170a | *Inorg. Chem.* 2012, 51, 13114−13122

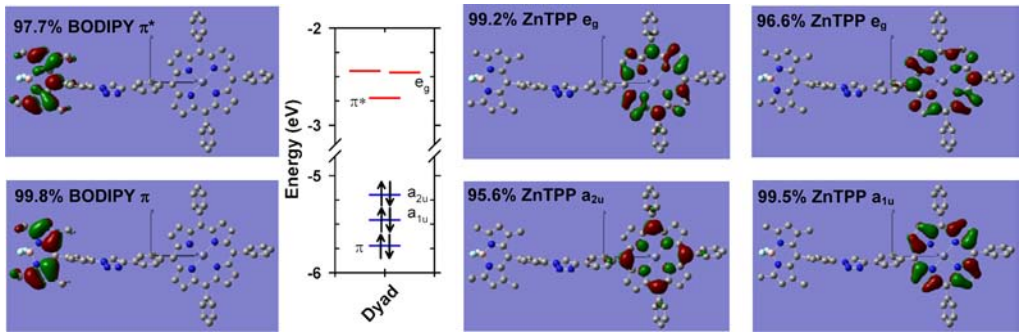

Figure 6. Frontier molecular orbitals for the **Dyad** calculated at the B3LYP/6-311g(2d,p)/PCM(THF) level of theory. The symmetry labels correspond to the Gouterman orbitals associated with the Soret and Q-bands electronic transitions. Included in the plot are orbital composition percentages estimated from the individual fragments.

more efficient transfer. There is also a slight trend of decreasing lifetime with increasing number of BODIPY attachments. This can be attributed to the additional substitution of the triazole on the *para* position of the porphyrin phenyl ring allowing more rotational freedom.[37]

Electronic Structure Calculations. Density functional theory electronic structure calculations were performed on the **Dyad**, **Tetrad**, **Pentad**, and individual chromophores to assist in understanding the EnT pathways for the arrays. All structures were optimized in the gas phase at the B3LYP/6-31g(d) level of theory.[38−42] The optimized structures show two low energy conformations of the BODIPY with respect to the plane of the porphyrin as a result of rotation about the phenyl-1,4-triazole-phenyl linkage. The two conformations place the BODIPY plane at about ∼0 and ∼30 degrees with respect to the porphyrin ring.

The gas phase geometry optimized structures were followed by B3LYP/6-311g(2d,p) single point calculations utilizing the self-consistent reaction field (SCRF) method with the polarizable continuum model (PCM)[43] approach to estimate the solvation effect of THF. Figure 6 shows the frontier molecular orbitals for the **Dyad** (HOMO −2 to LUMO +2). Frontier molecular orbitals of the remaining complexes are included in the Supporting Information. Included in Figure 6 are the percent orbital compositions based on the fragment analysis using the AOMix software for the 5,10,15-(triphenyl)-porphyrin Zn(II), phenyl-1,4-triazole-phenyl linkage, and BODIPY. The orbital contributions clearly show localization of the four Gouterman orbitals of the porphyrin (HOMO −1 a_{1u}, HOMO a_{2u}, LUMO +1 e_g, and LUMO +2 e_g) from the BODIPY π-system (HOMO −2, LUMO). The localization of the porphyrin and BODIPY orbitals and the lack of significant mixing through the phenyl-1,4-triazole-phenyl linkage support the assignment of the Förster mechanism (through space dipole−dipole)[26] for EnT between chromophores, as opposed to Dexter (through-bond).[44] Comparison of the **Tetrad** and **Pentad** molecular orbitals shows similar isolation of the ZnTPP and BODIPY chromophore π-systems (Supporting Information).

Figure 7 shows the comparison of frontier MO energy levels for the arrays and individual building blocks obtained from the B3LYP/6-311g(2d,p)/PCM calculations. Occupied orbitals are shown in blue and unoccupied in red. The dashed gray lines link the corresponding orbitals for the Gouterman 4-orbital model of the porphyrin and the BODIPY π system. Incorporation of the 1,2,3-triazoles in the structures lowers the energy levels of all the chromophores slightly but does not

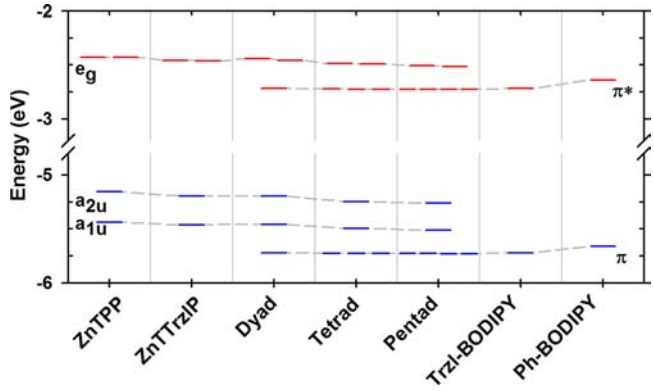

Figure 7. Plot of the frontier molecular orbital energy levels for all complexes examined in this work. Occupied orbitals are shown in blue and unoccupied in red. The dashed gray lines link the corresponding orbitals for the Gouterman four-orbital model of the porphyrin and the BODIPY π system.

have a large influence on the gap between them. In all systems, the interaction between the porphyrin Gouterman orbitals and BODIPY π system is essentially nonexistent.

To further elucidate the Förster interaction between BODIPY and ZnTPP in the **Dyad**, time-dependent density functional theory (TDDFT)[45,46] at B3LYP/6-311g(2d,p) level of theory, with PCM (THF), was applied to calculate the singlet excited states. The TDDFT results qualitatively reproduce the visible absorption spectra of the **Dyad**. Figure 8 shows the visible absorption spectra of the **Dyad** in THF along with the electronic transitions predicted by TDDFT. All of the main singlet transitions of the **Dyad** are reproduced by the TDDFT results, but the energetics are slightly shifted. The TDDFT results predict the Q-band transitions for the porphyrin and $\pi-\pi^*$ for the BODIPY at higher energies, while the Soret band at lower energies.

Singlet Energy Transfer Analysis. Fluorescence emission and excitation spectra shown above in Figures 4 and 5 show clear evidence of EnT from the BODIPY donors to the ZnTPP based acceptors for the three arrays. To analyze the efficiency of EnT in these systems, we compared the fluorescence spectra of the individual chromophores to that of the arrays. Figure 9 shows the emission spectra of the **Dyad** and an equimolar solution of **Trzl-BODIPY** and **ZnTPP** (both samples had an absorption of 0.1 at the BODIPY maximum of 502 nm). The emission band from BODIPY is quenched almost 10-fold in the **Dyad** as compared to the free BODIPY. Using eq 1, we can

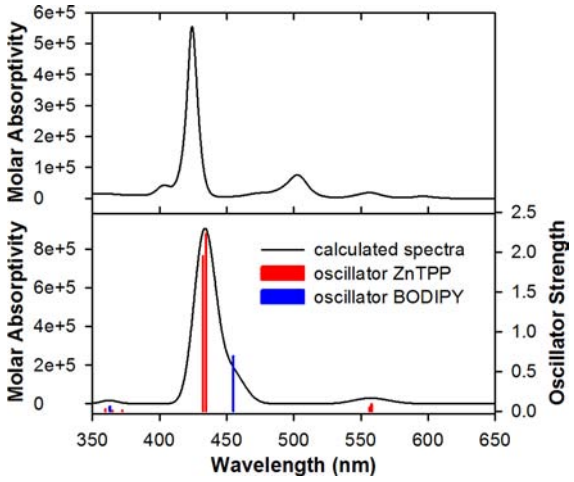

Figure 8. Comparison of absorbance and TDDFT spectra of **Dyad**. Top: Absorption spectra of the **Dyad** in THF. Bottom: Simulated spectra of the **Dyad** from TDDFT calculations at the B3LYP/6-311g(2d,p)/PCM(THF) level of theory. The simulated absorption spectra were generated using a 1000 cm^{-1} bandwidth for all peaks. The solid vertical lines correspond to the oscillator strengths of the calculated singlet transitions.

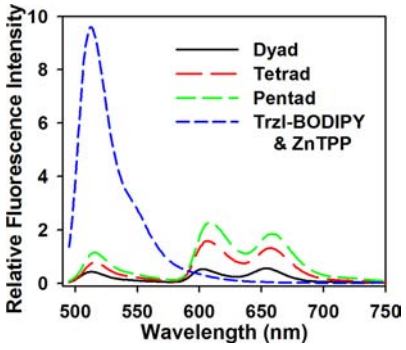

Figure 9. Emission spectra of the **Dyad**, **Tetrad**, **Pentad**, and an equimolar solution of **Trzl-BODIPY** and **ZnTPP** in THF excited at 495 nm. Both samples had an absorption of 0.1 at the BODIPY maximum of 502 nm.

calculate the efficiency of EnT through quenching of the BODIPY emission.

$$\mathrm{EnT}(\%) = \left[1 - \frac{F_{DA}}{F_D}\right] \times 100\% \quad (1)$$

In eq 1, F_{DA} and F_D are the fluorescence intensity of the donor in the presence and absence of the acceptor, respectively. Using the integrated emission spectra for the arrays and normalizing for the number of donor BODIPY units, we calculate EnT efficiencies of 95.8, 97.5, and 97.2% for the **Dyad**, **Tetrad**, and **Pentad** respectively (Table 2).

Förster theory[26] can be applied to the photophysical data of the arrays and BODIPY donor to estimate the rates and yield of EnT between chromophores. The Förster radius in Å (R_o, the distance at which the EnT efficiency is 50%) is given by eq 2:

$$R_o^6 = 8.79 \times 10^{-5}\left(\frac{\phi_D \kappa^2}{n^4}\right)\frac{\int_0^\infty F_D(\lambda)\varepsilon_A(\lambda)\lambda^4\, d\lambda}{\int_0^\infty F_D(\lambda)\, d\lambda} \quad (2)$$

where ϕ_D is the quantum yield of the BODIPY donor in the absence of the ZnTPP acceptor and n is the refractive index of the solvent. The integrals on the right side of eq 2 represent the overlap integral (J_F in M^{-1} cm^{-1} nm^4) of the donor emission spectra ($F_D(\lambda)$) and the acceptor absorption profile ($\varepsilon_A(\lambda)$). As shown in Figure 3, the emission spectra of **BODIPY** has good overlap with the Q-band absorptions for **ZnTTrzlP**. The calculated values of J_F for the three arrays, shown in Table 2, were calculated using the emission profile of **Trzl-BODIPY** and the Q-band absorption features of the **Dyad**, **Tetrad**, and **Pentad**. The slight red-shift in absorption peaks for the **Tetrad** with respect to the **Dyad** leads to a decrease in J_F, but the higher absorptivity of the **Pentad** results in the highest J_F of the three.

Table 2. EnT Efficiencies and Förster Overlap Integral and Distances for the Arrays

compound	experimental EnT %[a]	J_F (M^{-1} cm^{-1} nm^4)	R_0 (Å)[b]	FRET %[c]
Dyad	95.8	2.67×10^{14}	29.6	96.4
Tetrad	97.5	2.61×10^{14}	29.5	96.4
Pentad	97.2	3.02×10^{14}	30.2	96.8

[a]Calculated via eq 1. [b]Calculated via eq 2. [c]Calculated via eq 4.

Finally, κ^2 in eq 2 is an orientation factor describing the relative orientation of the electronic dipole moments of the associated transitions of the donor and acceptor corresponding to FRET. Typically, a value of 2/3 is used for κ^2, which assumes an average isotropic distribution of dipole arrangements. From the TDDFT results of the **Dyad**, we can determine a precise value of κ^2 using the calculated transition dipole moments from eq 3.

$$\kappa^2 = (\sin\theta_D \sin\theta_A \cos\Phi - 2\cos\theta_D \cos\theta_A)^2 \quad (3)$$

In eq 3, θ_D and θ_A are the angles between donor emission and acceptor absorption transition moments and the vector joining the two, and Φ is the dihedral angle between the two transition dipoles. The TDDFT calculated transition dipole moment for the 455 nm BODIPY $\pi-\pi^*$ is oriented vertically, from one pyrrole ring to the other and is consistent with previous measurements.[47] The porphyrin acceptor is considered a planar oscillator due to the degenerate E_u state giving rise to the Q-band transitions.[48] The lowest DFT energy conformation of the **Dyad** places the BODIPY transition dipole moment in a nearly parallel orientation with the porphyrin plane, resulting in the highest possible κ^2 value. Rotations of the BODIPY chromophore relative to the porphyrin plane are expected due to a low barrier for meso-phenyl rotation of porphyrins.[49] Additional rotations can be expected by the phenyl-triazole-phenyl linker joining the porphyrin and BODIPY chromophores. Therefore, without an accurate knowledge of the weighted distribution of conformations, we calculated the dynamic average $\langle\kappa^2\rangle$ = 0.24 assuming all possible values of Φ.[50] This value is similar to *p,p′*-diarylethyne linked BODIPY-ZnTPP arrays studied by Lindsey and co-workers.[12]

The Förster radii (R_o) for all three arrays calculated from eq 2 are approximately 30 Å (Table 2) and are almost twice the distance between centers of the chromophore arrays (r) of 17.1 Å determined from the DFT structures. Additionally, once the Förster radii are determined, the efficiency of FRET (E_{FRET}%) within the systems can be estimated from eq 4.

$$E_{FRET}(\%) = \left[\frac{R_o^6}{R_o^6 + r^6}\right] \times 100\% \quad (4)$$

dx.doi.org/10.1021/ic301170a | *Inorg. Chem.* 2012, 51, 13114−13122

The E_{FRET}% values for the three arrays are incuded in Table 2 and are very close to the observed EnT efficiencies determined from fluorescence quenching of the BODIPY chromophore. The close match between the predicted and observed EnT efficiencies suggests that the Förster mechanism plays a dominant role in the three arrays.

CONCLUSIONS

CuAAC reactivity was successfully employed to synthesize three donor−acceptor EnT arrays that contain one (**Dyad**), three (**Tetrad**), and four (**Pentad**) BODIPY donors connected to a Zn-tetraphenylporphyrin acceptor. Photophysical characterization and DFT electronic structure modeling of the three arrays are consistent with efficient Förster resonance energy transfer from the BODIPY donors to the Zn-tetraphenylporphyrin acceptor. The BODIPY singlet excited state emission is efficiently quenched in all three arrays, leading to EnT efficiencies of greater than 95% in all three systems. Applying Förster theory to the spectroscopic data of the chromophores gives EnT efficiency estimates that are in close agreement with experimental values. While we cannot rule out contributions from a through-bond mechanism, comparison of the theoretical and measured EnT efficiencies suggests the through-space mechanism plays a dominant role in the three arrays. The three array systems studied here highlight the utility of the CuAAC reaction to create hierarchical structures to study EnT processes and potentially create molecular systems for solar energy conversion and artificial photosynthesis.

EXPERIMENTAL SECTION

General Methods. NMR spectra were obtained on a Varian 500 MHz spectrometer and the chemical shifts were referenced to that of the solvent. LR and HR MALDI-TOF MS were obtained on a Bruker Ultraflex III. LR and HR ESI MS were obtained on a Thermo Electron Finnigan TSQ Quantum Ultra. FTIR were obtained on a Thermo Nicolet 4700.

Materials. Solvents, ACS Reagent grade or better, were purchased from Sigma Aldrich or Fisher Scientific and used as received. Anhydrous THF (unstabilized) and dichloromethane (DCM) were dried by recirculating the nitrogen-purged solvent through a solid-state column purification system[51] (Vacuum Atmospheres Company, Hawthorne, CA) prior to use. THF for spectroscopic studies was stored in a Schlenk flask and was routinely check for peroxides and vacuum distilled immediately before use. Toluene was purged with nitrogen and dried over molecular sieves before use. 4-Azidobenzoic acid (Aldrich), benzylazide (Alfa Aesar), copper sulfate (Fisher Scientific), sodium ascorbate (Aldrich), and 2,5-di-*tert*-butylhydroquinone (Aldrich) were used as received. Zn(II) 5,10,15,20-tetra(4-ethynylphenyl)porphyrin (**1**)[52] and tris-(benzyltriazolylmethyl)amine (TBTA)[53] were synthesized according to literature methods. Zn(II) 5-(4-ethynylphenyl)-10,15,20-triphenyl porphyrin (**2**), and Zn(II) 5,10,15-(4-ethynylphenyl)-20-phenyl porphyrin (**3**) were synthesized via the Lindsey method[54,55] and Zn metalated and deprotected according to literature methods.[52] 5,10,15,20-Tetra-phenyl-porphyrin Zn(II) (**ZnTPP**) was donated by Prof. Alan Cutler and was purified by preparative TLC before each photophysical measurement.

4,4-Difluoro-8-(4-azidophenyl)-1,3,5,7-tetramethyl-4-bora-3a,4a-diaza-*s*-indacene (4). 4-Azidobenzoic acid (0.493 g, 3.02 mmol) was placed in a 50-mL round-bottom flask and the atmosphere was replaced with N_2. Twenty-five milliliters of dry DCM was added, and the mixture was stirred until a white suspension formed. Oxalyl chloride (0.4 mL, 5 mmol) was then added, followed by 3 drops of pyridine. The reaction mixture was shielded from light and left to stir at room temperature for 3 days, after which the reaction mixture had turned into an almost clear yellow solution. The solvent was evaporated under reduced pressure, leaving behind a yellow solid. Forty milliliters of dry DCM was then added to make a yellow solution which was then transferred via cannula to a flask containing a N_2 degassed solution of 0.622 mL of freshly distilled 2,4-dimethylpyrrole (0.5750 g, 6.04 mmol) in 28 mL of DCM. The mixture immediately turned a brown-orange color and was left to stir overnight. Then, 2.6 mL of triethylamine was added, and the solution was left to stir for 15 min, followed by the addition of 3 mL of boron trifluoride diethyl etherate, resulting in a dark green solution. After four additional hours of stirring, the reaction was opened to air and the organic layer was washed with three portions of saturated sodium bicarbonate, dried over $MgSO_4$, and the solvent was evaporated. The residue was then chromatographed on a silica column (DCM/hexanes 70:30) and the second band was collected. The purest fractions were concentrated to produce a dark orange viscous oil. Hexanes were added and the mixture was sonicated, producing an orange solid, which was then collected via vacuum filtration (160.3 mg, 14.6%). ^{1}H NMR ($CDCl_3$): δ 7.27 (d, 2H, phenyl), 7.16 (d, 2H, phenyl), 5.99 (s, 2H), 2.55 (s, 6H, CH_3), 1.42 (s, 6H, CH_3). HR-ESI: Calcd 365.1732, found 365.1734.

Dyad. 32 mg of **3** (0.046 mmol) and 18 mg of **4** (0.049 mmol) were dissolved in 16 mL of THF and the resulting solution was degassed with N_2. In a small microcentrifuge tube, a solution of 2 mg of $CuSO_4{\cdot}5H_2O$ (0.009 mmol) in 325 μL of H_2O was combined with a solution of 6 mg of TBTA (0.012 mmol) in 325 μL of DMSO to make a blue solution. To this was added a solution of 4 mg of 2,5-di-*tert*-butylhydroquinone (0.02 mmol) in 325 μL of THF. The mixture was briefly shaken and was quickly added to the porphyrin/BODIPY mixture via syringe. The reaction was heated to 40 °C and left to stir overnight. The mixture was cooled and the THF was evaporated to yield a reddish brown residue. Ten milliliters of methanol was added, giving a red-brown precipitate that was collected by filtration. This powder was then chromatographed on a preparatory-scale TLC plate (silica, DCM/MeOH 98:2). The second band from the top was collected and the product was extracted from the silica with DCM. The solution was filtered through glass wool and the solvent was evaporated to yield a dark purple solid (32 mg, 65%). ^{1}H NMR ($CDCl_3$): δ 9.03 (d, 2H, porphyrin β-pyrrole), 8.98 (d, 2H, porphyrin β-pyrrole), 8.96 (s, 4H, porphyrin β-pyrrole), 8.58 (s, 1H, triazole-H), 8.36 (d, 2H, BODIPY phenyl), 8.32 (d, 2H, BODIPY phenyl), 8.23 (m, 6H, porphyrin phenyl), 8.12 (d, 2H, porphyrin phenyl), 7.76 (m, 9H, porphyrin phenyl), 7.59 (d, 2H, porphyrin phenyl), 6.06 (s, 2H, BODIPY), 2.60 (s, 6H, BODIPY CH_3), 1.53 (s, 6H, BODIPY CH_3). HR-ESI: Calcd 1065.3223, found 1065.3244.

Tetrad. Following a similar procedure as the **Dyad**, 20 mg of **2** (0.026 mmol) and 30 mg of **4** (0.081 mmol) were reacted with 4 mg of $CuSO_4{\cdot}5H_2O$ (0.016 mmol), 11 mg of TBTA (0.020 mmol) and 6 mg of di-*tert*-butylhydroquinone (0.025 mmol) to yield a red-brown solid (8 mg, 15.8%). ^{1}H NMR ($CDCl_3$): δ 9.07 (s, 4H, porphyrin β-pyrrole), 9.05 (d, 2H, porphyrin β-pyrrole), 9.00 (d, 2H, porphyrin β-pyrrole), 8.57 (s, 1H, triazole-H), 8.56 (s, 2H, triazole-H), 8.36 (d, 6H, BODIPY phenyl), 8.31 (d, 6H, BODIPY phenyl), 8.24 (d, 2H, porphyrin phenyl), 8.10 (d, 6H, porphyrin phenyl), 7.78 (m, 3H, porphyrin phenyl), 7.58 (d, 6H, porphyrin phenyl), 6.05 (s, 6H, BODIPY), 2.59 (s, 18H, BODIPY-CH_3), 1.52 (s, 18H, BODIPY-CH_3). HR-ESI: Calcd 1843.6584, found 1843.6572.

Pentad. Following a similar procedure as the **Dyad**, 18 mg of **1** (0.023 mmol) and 34 mg of **4** (0.092 mmol) were reacted with 5 mg of $CuSO_4{\cdot}5H_2O$ (0.019 mmol), 6 mg of TBTA (0.023 mmol), and 7 mg of 2,5-di-*tert*-butylhydroquinone (0.030 mmol) to yield a brown solid (24.5 mg, 48.4%). ^{1}H NMR ($CDCl_3$): δ 9.09 (s, 8H, porphyrin β-pyrrole), 8.58 (s, 4H, triazole-H), 8.38 (d, 8H, BODIPY phenyl), 8.34 (d, 8H, BODIPY phenyl), 8.12 (d, 8H, porphyrin phenyl), 7.59 (d, 8H, porphyrin phenyl), 6.05 (s, 8H, BODIPY), 2.60 (s, 24H, BODIPY CH_3), 1.53 (s, 24H, BODIPY CH_3). HR-ESI: Calcd 2232.82078, found 2232.82027.

4,4-Difluoro-8-(4-(phenyl-1,4-triazole)-phenyl)-1,3,5,7-tetramethyl-4-bora-3a,4a-diaza-*s*-indacene (Trzl-BODIPY). Twenty-four milligrams of **4** (0.646 mmol) was dissolved in 20 mL of THF. 8.0 μL of phenylacetylene was added and the solution was degassed with N_2. To this was added a solution of 3 mg of $CuSO_4{\cdot}5H_2O$ (0.013 mmol) and 9 mg of TBTA (0.017 mmol) in 800 μL of 1:1 H_2O/

dx.doi.org/10.1021/ic301170a | *Inorg. Chem.* 2012, 51, 13114−13122

DMSO. This was mixed with a solution of 7 mg of di-*tert*-butylhydroquinone in 400 μL of THF. The resulting slightly yellow solution was added to the BODIPY-phenylacetylene solution via syringe and the reaction was heated overnight at 40 °C. The mixture was cooled and the THF was evaporated. The residue was then dissolved in DCM, washed twice with H_2O, dried over Na_2SO_4, and the solvent was evaporated. The resulting residue was then chromatographed on a silica column (DCM/MeOH 99:1) and the product eluted as the third band. This was concentrated to yield an orange solid (11 mg, 36.1%). ^{1}H NMR ($CDCl_3$): δ 8.31 (s, 1H, triazole-H), 8.00 (d, 2H, BODIPY phenyl), 7.94 (d, 2H, BODIPY phenyl), 7.50 (m, 4H, phenyl), 7.41 (m, 1H, phenyl), 6.02 (s, 2H, BODIPY), 2.58 (s, 6H, BODIPY CH_3), 1.46 (s, 6H, BODIPY CH_3). ESI: Calcd 467.2202, found 467.2196.

5,10,15,20-Tetra-(*p*-benzyl-1,4-triazolephenyl)porphyrin Zn-(II) (ZnTTrzlP). Following a similar procedure as the **Dyad**, 102 mg of **1** (0.13 mmol) and 85 mg of benzylazide (0.64 mmol) in 50 mL of THF were reacted with 35 mg of $CuSO_4 \cdot 5H_2O$ (0.14 mmol) in 500 μL of H_2O and combined with a solution of 73 mg of TBTA (0.14 mmol) in 500 μL of DMSO to make a dark blue-green solution. To this was added a solution of 56 mg of 2,5-di-*tert*-butylhydroquinone (0.25 mmol) in 500 μL of THF. The mixture was briefly shaken and quickly added to the reaction mixture via syringe. The reaction was left to stir overnight. Slow addition of a 1:1 mixture of methanol/water to the reaction solution precipitated a dark solid which was filtered and rinsed with a 1:1 mixture of methanol/water several times. Purification on silica using a solution of DCM/MeOH 98:2 yielded a dark purple solid after removal of the solvent. ^{1}H NMR ($CDCl_3$): δ 8.916 (s, 8H, β-pyrrole), 8.215 (d, 8H, J = 8.07 Hz, ortho-phenyl), 8.145 (d 8H, J = 8.07 Hz, meta-phenyl), 7.920 (s, 4H, triazole-H), 7.391−7.446 (m, 20H, benzyl peaks), 5.684 (s, 8H, benzyl-H). MALDI-HSMS: Calcd 1304.416, found 1304.414.

Photophysical Methods. Electronic absorption spectra were taken on a Perkin-Elmer Lambda 950 spectrometer. Steady-state fluorescence and quantum yield measurements were carried out on a HORIBA Jobin Yvon FluoroLog-Tau3 spectrofluorometer using a right-angle detection method. Quantum yields were calculated using the comparative method. Only dilute solutions with maximum optical densities less than 0.09 past the excitation wavelength were used to minimize inner filter effects. For the arrays, an excitation wavelength of 507 nm was used, for **ZnTTrzlP**, an excitation of 545 nm; and for **Trzl-BODIPY**, 475 nm. Solutions were prepared in matched 10 mm optical path length fluorescence quartz cells. Spectroscopic grade solvents were used to prepare all solutions, with the exception of tetrahydrofuran. Unstabilized THF was tested for peroxides using a Quantofix Peroxide 100 test strip. All samples were purged with nitrogen. Absorption measurements were then taken using a Perkin-Elmer Lambda 950 UV/vis spectrometer. Additionally, absorbance measurements were taken after each fluorescence spectrum. A blank was recorded for absorption and fluorescence prior to the addition of sample compound. Every fluorescence spectrum was corrected for both instrument and lamp variations. Refractive index data for solvents have been taken into account. Wavelengths were kept in nanometers and emission peaks were completely integrated using Orgin 8 Pro. SigmaPlot was used to graph absorbance vs integrated fluorescence to obtain the gradients. Each sample was performed in triplicate with R^2 values greater than 0.99.

Fluorescence lifetimes were measured by phase modulated frequency-domain lifetime using a Horiba Spex FluoroLog-Tau3 spectrometer. To remove stray light and fluorescence from other sources, long pass filters were used on the detector side. A 550 nm long pass was used for BODIPY and a 600 long pass was used for the porphyrins and arrays. All solutions were purged with nitrogen gas to remove oxygen prior to steady-state and lifetime fluorescence measurements. A lifetime resolved model was used to fit the data. Data included in this report were the average of at least three measurements. A selection of phase-modulated data and fits are included in the Supporting Information.

Computational Details. Geometry optimizations for the porphyin-azido-linker constructs were carried out using density functional theory (DFT) as implemented in Gaussian03, revision E.01.[56] Becke's three-parameter hybrid functional[38−41] with the LYP correlation functional[42] (B3LYP) was used with the 6-31g(d) basis set for geometry optimizations in the gas phase. The **Dyad**, **Tetrad**, **Ph-BODIPY**, and **Trzl-BODIPY** were optimized without symmetry constraints, whereas the **Pentad** was done under the D_2 point group. Single point energy and TDDFT calculations were performed on the gas-phase optimized structure at the B3LYP/6-311g(2d,p) level of theory and included the effect of solvation by THF using the self-consistent reaction field (SCRF) of polarizable continuum model (PCM)[43] approach. Molecular orbital compositions and overlap populations were calculated by employing the AOMix program.[57,58] The analysis of the MO compositions in terms of occupied and unoccupied fragment molecular orbitals, the charge decomposition analysis, and the construction of orbital interaction diagrams were performed by using AOMix-CDA.[59]

■ ASSOCIATED CONTENT

Ⓢ Supporting Information

Synthetic scheme for **4**, quantum yield data, a selection of phase-modulated singlet lifetime data and fitting, images of the frontier molecular orbitals for the arrays and individual chromophores, and TDDFT singlet state energies for the **Dyad**. This material is available free of charge via the Internet at http://pubs.acs.org.

■ AUTHOR INFORMATION

Corresponding Author

*E-mail: dinolp@rpi.edu.

Present Address

†Department of Chemistry, Northwestern University, Evanston, IL 60208.

Notes

The authors declare no competing financial interest.

■ ACKNOWLEDGMENTS

This work was supported by Rensselaer Polytechnic Institute through new faculty start-up funds. M.R.T. acknowledges a Wiseman Family Fellowship from Rensselaer Polytechnic Institute, and M.J.L. acknowledges an Arthur G. Schultz Award for Undergraduate Research in Organic Chemistry.

■ REFERENCES

(1) Hambourger, M.; Moore, G. F.; Kramer, D. M.; Gust, D.; Moore, A. L.; Moore, T. A. *Chem. Soc. Rev.* **2009**, *38*, 25−35.

(2) Benniston, A. C.; Harriman, A. *Mater. Today* **2008**, *11*, 26−34.

(3) Gust, D.; Moore, T. A.; Moore, A. L. *Acc. Chem. Res.* **2000**, *34*, 40−48.

(4) Meyer, T. J. *Acc. Chem. Res.* **1989**, *22*, 163−170.

(5) Wasielewski, M. R. *Chem. Rev.* **1992**, *92*, 435−461.

(6) Treibs, A.; Kreuzer, F. H. *Justus Liebigs Ann. Chem.* **1968**, *718*, 208−223.

(7) Loudet, A.; Burgess, K. *Chem. Rev.* **2007**, *107*, 4891−4932.

(8) Chen, Y.; Wan, L.; Yu, X.; Li, W.; Bian, Y.; Jiang, J. *Org. Lett.* **2011**, *13*, 5774−5777.

(9) Lazarides, T.; Charalambidis, G.; Vuillamy, A.; Réglier, M.; Klontzas, E.; Froudakis, G.; Kuhri, S.; Guldi, D. M.; Coutsolelos, A. G. *Inorg. Chem.* **2011**, *50*, 8926−8936.

(10) Wu, W.; Guo, H.; Wu, W.; Ji, S.; Zhao, J. *J. Org. Chem.* **2011**, *76*, 7056−7064.

(11) Koepf, M.; Trabolsi, A.; Elhabiri, M.; Wytko, J. A.; Paul, D.; Albrecht-Gary, A. M.; Weiss, J. *Org. Lett.* **2005**, *7*, 1279−1282.

(12) Li, F.; Yang, S. I.; Ciringh, Y.; Seth, J.; Martin, C. H.; Singh, D. L.; Kim, D.; Birge, R. R.; Bocian, D. F.; Holten, D.; Lindsey, J. S. *J. Am. Chem. Soc.* **1998**, *120*, 10001−10017.

(13) Ambroise, A.; Kirmaier, C.; Wagner, R. W.; Loewe, R. S.; Bocian, D. F.; Holten, D.; Lindsey, J. S. *J. Org. Chem.* **2002**, *67*, 3811−3826.
(14) Wagner, R. W.; Lindsey, J. S. *J. Am. Chem. Soc.* **1994**, *116*, 9759−9760.
(15) Lee, C. Y.; Hupp, J. T. *Langmuir* **2010**, *26*, 3760−3765.
(16) Warnan, J.; Buchet, F.; Pellegrin, Y.; Blart, E.; Odobel, F. *Org. Lett.* **2011**, *13*, 3944−3947.
(17) Gu, Z.-Y.; Guo, D.-S.; Sun, M.; Liu, Y. *J. Org. Chem.* **2010**, *75*, 3600−3607.
(18) Lee, C. Y.; Farha, O. K.; Hong, B. J.; Sarjeant, A. A.; Nguyen, S. T.; Hupp, J. T. *J. Am. Chem. Soc.* **2011**, *133*, 15858−15861.
(19) Kolb, H. C.; Finn, M. G.; Sharpless, K. B. *Angew. Chem., Int. Ed.* **2001**, *40*, 2004−2021.
(20) Rostovtsev, V. V.; Green, L. G.; Fokin, V. V.; Sharpless, K. B. *Angew. Chem., Int. Ed.* **2002**, *41*, 2596−2599.
(21) Meldal, M.; Tornøe, C. W. *Chem. Rev.* **2008**, *108*, 2952−3015.
(22) Palomaki, P. K. B.; Krawicz, A.; Dinolfo, P. H. *Langmuir* **2011**, *27*, 4613−4622.
(23) Palomaki, P. K. B.; Dinolfo, P. H. *Langmuir* **2010**, *26*, 9677−9685.
(24) Palomaki, P. K. B.; Dinolfo, P. H. *ACS Appl. Mater. Interfaces* **2011**, *3*, 4703−4713.
(25) Krawicz, A.; Palazzo, J.; Wang, G. C.; Dinolfo, P. H. *RCS Advances* **2012**, *2*, 7513−7522.
(26) Förster, T. *Naturwissenschaften* **1946**, *33*, 166−175.
(27) Kollmannsberger, M.; Rurack, K.; Resch-Genger, U.; Daub, J. *J. Phys. Chem. A* **1998**, *102*, 10211−10220.
(28) Wagner, R. W.; Lindsey, J. S. *Pure Appl. Chem.* **1996**, *68*, 1373−1380.
(29) Weinkauf, J. R.; Cooper, S. W.; Schweiger, A.; Wamser, C. C. *J. Phys. Chem. A* **2002**, *107*, 3486−3496.
(30) Yaochuan, W.; Dakui, Z.; Hui, Z.; Jinliang, D.; Qiang, C.; Yi, X.; Shixiong, Q. *J. Appl. Phys.* **2010**, *108*, 033520.
(31) Qin, W.; Baruah, M.; Van der Auweraer, M.; De Schryver, F. C.; Boens, N. *J. Phys. Chem. A* **2005**, *109*, 7371−7384.
(32) Li, Y.; Cao, L.; Tian, H. *J. Org. Chem.* **2006**, *71*, 8279−8282.
(33) Zhu, L.-J.; Wang, J.; Reng, T.-G.; Li, C.-Y.; Guo, D.-C.; Guo, C.-C. *J. Phys. Org. Chem.* **2010**, *23*, 1099−1395.
(34) Wang, D. C., X.; Shi, Y.; Sun, E.; Tang, X.; Zhuang, C.; Shi, T. *Solid State Sci.* **2009**, *11*, 195−199.
(35) Lahann, J. *Click Chemistry for Biotechnology and Materials Science*; John Wiley & Sons, Ltd: New York, 2009.
(36) Rajesh, C. S.; Capitosti, G. J.; Cramer, S. J.; Modarelli, D. A. *J. Phys. Chem. B* **2001**, *105*, 10175−10188.
(37) Berezin, M. Y.; Achilefu, S. *Chem. Rev.* **2010**, *110*, 2641−2684.
(38) Becke, A. D. *Phys. Rev. A* **1988**, *38*, 3098−3100.
(39) Becke, A. D. *J. Chem. Phys.* **1993**, *98*, 1372−1377.
(40) Becke, A. D. *J. Chem. Phys.* **1993**, *98*, 5648−5652.
(41) Stephens, P. J.; Devlin, F. J.; Chabalowski, C. F.; Frisch, M. J. *J. Phys. Chem.* **1994**, *98*, 11623−11627.
(42) Lee, C.; Yang, W.; Parr, R. G. *Phys. Rev. B* **1988**, *37*, 785−789.
(43) Miertus, S.; Tomasi, J. *Chem. Phys.* **1982**, *65*, 239−245.
(44) Dexter, D. L. *J. Chem. Phys.* **1953**, *21*, 836−850.
(45) Runge, E.; Gross, E. K. U. *Phys. Rev. Lett.* **1984**, *52*, 997−1000.
(46) Casida, M. E. *Recent Advances in Density Functional Methods*; World Scientific: Singapore, 1995.
(47) Karolin, J.; Johansson, L. B. A.; Strandberg, L.; Ny, T. *J. Am. Chem. Soc.* **1994**, *116*, 7801−7806.
(48) Gurinovich, G. P.; Sevchenko, A. N.; Solv'ev, K. N. *Opt. Spectrosc.* **1961**, *10*, 396−401.
(49) Kottas, G. S.; Clarke, L. I.; Horinek, D.; Michl, J. *Chem. Rev.* **2005**, *105*, 1281−1376.
(50) Mårtensson, J. *Chem. Phys. Lett.* **1994**, *229*, 449−456.
(51) Pangborn, A. B.; Giardello, M. A.; Grubbs, R. H.; Rosen, R. K.; Timmers, F. J. *Organometallics* **1996**, *15*, 1518−1520.
(52) Onitsuka, K.; Kitajima, H.; Fujimoto, M.; Iuchi, A.; Takei, F.; Takahashi, S. *Chem. Commun.* **2002**, 2576−2577.
(53) Chan, T. R.; Hilgraf, R.; Sharpless, K. B.; Fokin, V. V. *Org. Lett.* **2004**, *6*, 2853−2855.
(54) Lee, C.-H.; S. Lindsey, J. *Tetrahedron* **1994**, *50*, 11427−11440.
(55) Baker, G. A.; Bright, F. V.; Detty, M. R.; Pandey, S.; Stilts, C. E.; Yao, H. *J. Porphyrins Phthalocyanines* **2000**, *4*, 669−683.
(56) *Gaussian 03*, Revision E.01; Frisch, M. J.; Trucks, G. W.; Schlegel, H. B.; Scuseria, G. E.; Robb, M. A.; Cheeseman, J. R.; Montgomery, J., J., A.; Vreven, T.; Kudin, K. N.; Burant, J. C.; Millam, J. M.; Iyengar, S. S.; Tomasi, J.; Barone, V.; Mennucci, B.; Cossi, M.; Scalmani, G.; Rega, N.; Petersson, G. A.; Nakatsuji, H.; Hada, M.; Ehara, M.; Toyota, K.; Fukuda, R.; Hasegawa, J.; Ishida, M.; Nakajima, T.; Honda, Y.; Kitao, O.; Nakai, H.; Klene, M.; Li, X.; Knox, J. E.; Hratchian, H. P.; Cross, J. B.; Bakken, V.; Adamo, C.; Jaramillo, J.; Gomperts, R.; Stratmann, R. E.; Yazyev, O.; Austin, A. J.; Cammi, R.; Pomelli, C.; Ochterski, J. W.; Ayala, P. Y.; Morokuma, K.; Voth, G. A.; Salvador, P.; Dannenberg, J. J.; Zakrzewski, V. G.; Dapprich, S.; Daniels, A. D.; Strain, M. C.; Farkas, O.; Malick, D. K.; Rabuck, A. D.; Raghavachari, K.; Foresman, J. B.; Ortiz, J. V.; Cui, Q.; Baboul, A. G.; Clifford, S.; Cioslowski, J.; Stefanov, B. B.; Liu, G.; Liashenko, A.; Piskorz, P.; Komaromi, I.; Martin, R. L.; Fox, D. J.; Keith, T.; Al-Laham, M. A.; Peng, C. Y.; Nanayakkara, A.; Challacombe, M.; Gill, P. M. W.; Johnson, B.; Chen, W.; Wong, M. W.; Gonzalez, C.; Pople, J. A. Gaussian, Inc.: Wallingford, CT, 2004.
(57) Gorelsky, S. I.; Lever, A. B. P. *J. Organomet. Chem.* **2001**, *635*, 187−196.
(58) Gorelsky, S. I. *AOMix: Program for Molecular Orbital Analysis*, 6.54; York University: Toronto, Canada, 1997.
(59) Gorelsky, S. I.; Ghosh, S.; Solomon, E. I. *J. Am. Chem. Soc.* **2005**, *128*, 278−290.